Eur. Phys. J. C 50, 283–297 (2007)
DOI 10.1140/epjc/s10052-007-0241-7

THE EUROPEAN PHYSICAL JOURNAL C

Regular Article – Experimental Physics

Photoproduction of events with rapidity gaps between jets at HERA

The ZEUS Collaboration

S. Chekanov[1,a], M. Derrick[1], S. Magill[1], S. Miglioranzi[1,53], B. Musgrave[1], D. Nicholass[1,53], J. Repond[1], R. Yoshida[1], M.C.K. Mattingly[2], N. Pavel[3,b], A.G.Y. Molina[3], S. Antonelli[4], P. Antonioli[4], G. Bari[4], M. Basile[4], L. Bellagamba[4], M. Bindi[4], D. Boscherini[4], A. Bruni[4], G. Bruni[4], L. Cifarelli[4], F. Cindolo[4], A. Contin[4], M. Corradi[4,54,c], S. De Pasquale[4], G. Iacobucci[4], A. Margotti[4], R. Nania[4], A. Polini[4], L. Rinaldi[4], G. Sartorelli[4], A. Zichichi[4], G. Aghuzumtsyan[5,d], D. Bartsch[5], I. Brock[5], S. Goers[5], H. Hartmann[5], E. Hilger[5], H.-P. Jakob[5], M. Jüngst[5], O.M. Kind[5], E. Paul[5,e], J. Rautenberg[5,55], R. Renner[5], U. Samson[5,f], V. Schönberg[5], M. Wang[5], M. Wlasenko[5], N.H. Brook[6], G.P. Heath[6], J.D. Morris[6], T. Namsoo[6], M. Capua[7], S. Fazio[7], A. Mastroberardino[7], M. Schioppa[7], G. Susinno[7], E. Tassi[7], J.Y. Kim[8,g], K.J. Ma[8,h], Z.A. Ibrahim[9], B. Kamaluddin[9], W.A.T.W. Abdullah[9], Y. Ning[10], Z. Ren[10], F. Sciulli[10], J. Chwastowski[11], A. Eskreys[11], J. Figiel[11], A. Galas[11], M. Gil[11], K. Olkiewicz[11], P. Stopa[11], L. Zawiejski[11], L. Adamczyk[12], T. Bołd[12], I. Grabowska-Bołd[12], D. Kisielewska[12], J. Łukasik[12], M. Przybycień[12], L. Suszycki[12], A. Kotański[13,i], W. Słomiński[13], V. Adler[14], U. Behrens[14], I. Bloch[14], A. Bonato[14], K. Borras[14], N. Coppola[14], J. Fourletova[14], A. Geiser[14], D. Gladkov[14], P. Göttlicher[14,56], I. Gregor[14], T. Haas[14], W. Hain[14], C. Horn[14], B. Kahle[14], U. Kötz[14], H. Kowalski[14], E. Lobodzinska[14], B. Löhr[14], R. Mankel[14], I.-A. Melzer-Pellmann[14], A. Montanari[14], D. Notz[14], A.E. Nuncio-Quiroz[14], R. Santamarta[14], U. Schneekloth[14], A. Spiridonov[14,57], H. Stadie[14], U. Stösslein[14], D. Szuba[14,58], J. Szuba[14,j], T. Theedt[14], G. Wolf[14], K. Wrona[14], C. Youngman[14], W. Zeuner[14], S. Schlenstedt[15], G. Barbagli[16], E. Gallo[16,k], P.G. Pelfer[16], A. Bamberger[17], D. Dobur[17], F. Karstens[17], N.N. Vlasov[17,l], P.J. Bussey[18], A.T. Doyle[18], W. Dunne[18], J. Ferrando[18], D.H. Saxon[18], I.O. Skillicorn[18], I. Gialas[19,66], T. Gosau[20], U. Holm[20], R. Klanner[20], E. Lohrmann[20], H. Salehi[20], P. Schleper[20], T. Schörner-Sadenius[20], J. Sztuk[20], K. Wichmann[20], K. Wick[20], C. Foudas[21], C. Fry[21], K.R. Long[21], A.D. Tapper[21], M. Kataoka[22,59], T. Matsumoto[22], K. Nagano[22], K. Tokushuku[22,60], S. Yamada[22], Y. Yamazaki[22], A.N. Barakbaev[23], E.G. Boos[23], A. Dossanov[23], N.S. Pokrovskiy[23], B.O. Zhautykov[23], D. Son[24], J. de Favereau[25], K. Piotrzkowski[25], F. Barreiro[26], C. Glasman[26,m], M. Jimenez[26], L. Labarga[26], J. del Peso[26], E. Ron[26], J. Terrón[26], M. Zambrana[26], F. Corriveau[27], C. Liu[27], R. Walsh[27], C. Zhou[27], T. Tsurugai[28], A. Antonov[29], B.A. Dolgoshein[29], I. Rubinsky[29], V. Sosnovtsev[29], A. Stifutkin[29], S. Suchkov[29], R.K. Dementiev[30], P.F. Ermolov[30], L.K. Gladilin[30], I.I. Katkov[30], L.A. Khein[30], I.A. Korzhavina[30], V.A. Kuzmin[30], B.B. Levchenko[30,n], O.Y. Lukina[30], A.S. Proskuryakov[30], L.M. Shcheglova[30], D.S. Zotkin[30], S.A. Zotkin[30], I. Abt[31], C. Büttner[31], A. Caldwell[31], D. Kollar[31], W.B. Schmidke[31], J. Sutiak[31], G. Grigorescu[32], A. Keramidas[32], E. Koffeman[32], P. Kooijman[32], A. Pellegrino[32], H. Tiecke[32], M. Vázquez[32,61], L. Wiggers[32], N. Brümmer[33], B. Bylsma[33], L.S. Durkin[33], A. Lee[33], T.Y. Ling[33], P.D. Allfrey[34], M.A. Bell[34], A.M. Cooper-Sarkar[34], A. Cottrell[34], R.C.E. Devenish[34], B. Foster[34], K. Korcsak-Gorzo[34], S. Patel[34], V. Roberfroid[34,o], A. Robertson[34], P.B. Straub[34], C. Uribe-Estrada[34], R. Walczak[34], P. Bellan[35], A. Bertolin[35], R. Brugnera[35], R. Carlin[35], R. Ciesielski[35], F. Dal Corso[35], S. Dusini[35], A. Garfagnini[35], S. Limentani[35], A. Longhin[35], L. Stanco[35], M. Turcato[35], B.Y. Oh[36], A. Raval[36], J. Ukleja[36,p], J.J. Whitmore[36], Y. Iga[37], G. D'Agostini[38], G. Marini[38], A. Nigro[38], J.E. Cole[39], J.C. Hart[39], H. Abramowicz[40,62,q], A. Gabareen[40], R. Ingbir[40], S. Kananov[40], A. Levy[40], M. Kuze[41], R. Hori[42], S. Kagawa[42,r], S. Shimizu[42], T. Tawara[42], R. Hamatsu[43], H. Kaji[43], S. Kitamura[43,63], O. Ota[43], Y.D. Ri[43], M.I. Ferrero[44], V. Monaco[44], R. Sacchi[44], A. Solano[44], M. Arneodo[45], M. Ruspa[45], S. Fourletov[46], J.F. Martin[46], S.K. Boutle[47,66], J.M. Butterworth[47], C. Gwenlan[47,s], T.W. Jones[47], J.H. Loizides[47], M.R. Sutton[47,q], C. Targett-Adams[47], M. Wing[47], B. Brzozowska[48], J. Ciborowski[48,64], G. Grzelak[48], P. Kulinski[48], P. Łużniak[48,65], J. Malka[48,65], R.J. Nowak[48], J.M. Pawlak[48], T. Tymieniecka[48], A. Ukleja[48,t], A.F. Żarnecki[48], M. Adamus[49], P. Plucinski[49,u], Y. Eisenberg[50], I. Giller[50], D. Hochman[50], U. Karshon[50], M. Rosin[50], E. Brownson[51], T. Danielson[51], A. Everett[51], D. Kçira[51], D.D. Reeder[51], P. Ryan[51], A.A. Savin[51], W.H. Smith[51], H. Wolfe[51], S. Bhadra[52], C.D. Catterall[52], Y. Cui[52], G. Hartner[52], S. Menary[52], U. Noor[52], M. Soares[52], J. Standage[52], J. Whyte[52]

[1] Argonne National Laboratory, Argonne, Illinois 60439-4815, USA[v]
[2] Andrews University, Berrien Springs, Michigan 49104-0380, USA
[3] Institut für Physik der Humboldt-Universität zu Berlin, Berlin, Germany
[4] University and INFN Bologna, Bologna, Italy[w]
[5] Physikalisches Institut der Universität Bonn, Bonn, Germany[x]

[6] H.H. Wills Physics Laboratory, University of Bristol, Bristol, UK[y]
[7] Calabria University, Physics Department and INFN, Cosenza, Italy[w]
[8] Chonnam National University, Kwangju, South Korea[z]
[9] Jabatan Fizik, Universiti Malaya, 50603 Kuala Lumpur, Malaysia[aa]
[10] Nevis Laboratories, Columbia University, Irvington on Hudson, New York 10027, USA[ab]
[11] The Henryk Niewodniczanski Institute of Nuclear Physics, Polish Academy of Sciences, Cracow, Poland[ac]
[12] Faculty of Physics and Applied Computer Science, AGH-University of Science and Technology, Cracow, Poland[ad]
[13] Department of Physics, Jagellonian University, Cracow, Poland
[14] Deutsches Elektronen-Synchrotron DESY, Hamburg, Germany
[15] Deutsches Elektronen-Synchrotron DESY, Zeuthen, Germany
[16] University and INFN, Florence, Italy[w]
[17] Fakultät für Physik der Universität Freiburg i. Br., Freiburg i. Br., Germany[x]
[18] Department of Physics and Astronomy, University of Glasgow, Glasgow, UK[y]
[19] Department of Engineering in Management and Finance, Univ. of Aegean, Greece
[20] Hamburg University, Institute of Exp. Physics, Hamburg, Germany[x]
[21] Imperial College London, High Energy Nuclear Physics Group, London, UK[y]
[22] Institute of Particle and Nuclear Studies, KEK, Tsukuba, Japan[al]
[23] Institute of Physics and Technology of Ministry of Education and Science of Kazakhstan, Almaty, Kazakhstan
[24] Kyungpook National University, Center for High Energy Physics, Daegu, South Korea[z]
[25] Institut de Physique Nucléaire, Université Catholique de Louvain, Louvain-la-Neuve, Belgium[ae]
[26] Departamento de Física Teórica, Universidad Autónoma de Madrid, Madrid, Spain[af]
[27] Department of Physics, McGill University, Montréal, Québec, Canada H3A 2T8[ag]
[28] Meiji Gakuin University, Faculty of General Education, Yokohama, Japan[al]
[29] Moscow Engineering Physics Institute, Moscow, Russia[ah]
[30] Moscow State University, Institute of Nuclear Physics, Moscow, Russia[ai]
[31] Max-Planck-Institut für Physik, München, Germany
[32] NIKHEF and University of Amsterdam, Amsterdam, Netherlands[aj]
[33] Physics Department, Ohio State University, Columbus, Ohio 43210, USA[v]
[34] Department of Physics, University of Oxford, Oxford, UK[y]
[35] Dipartimento di Fisica dell' Università and INFN, Padova, Italy[w]
[36] Department of Physics, Pennsylvania State University, University Park, Pennsylvania 16802, USA[ab]
[37] Polytechnic University, Sagamihara, Japan[al]
[38] Dipartimento di Fisica, Università 'La Sapienza' and INFN, Rome, Italy[w]
[39] Rutherford Appleton Laboratory, Chilton, Didcot, Oxon, UK[y]
[40] Raymond and Beverly Sackler Faculty of Exact Sciences, School of Physics, Tel-Aviv University, Tel-Aviv, Israel[ak]
[41] Department of Physics, Tokyo Institute of Technology, Tokyo, Japan[al]
[42] Department of Physics, University of Tokyo, Tokyo, Japan[al]
[43] Tokyo Metropolitan University, Department of Physics, Tokyo, Japan[al]
[44] Università di Torino and INFN, Torino, Italy[w]
[45] Università del Piemonte Orientale, Novara, and INFN, Torino, Italy[w]
[46] Department of Physics, University of Toronto, Toronto, Ontario, Canada M5S 1A7[ag]
[47] Physics and Astronomy Department, University College London, London, UK[y]
[48] Warsaw University, Institute of Experimental Physics, Warsaw, Poland
[49] Institute for Nuclear Studies, Warsaw, Poland
[50] Department of Particle Physics, Weizmann Institute, Rehovot, Israel[am]
[51] Department of Physics, University of Wisconsin, Madison, Wisconsin 53706, USA[v]
[52] Department of Physics, York University, Ontario, Canada M3J 1P3[ag]
[53] also affiliated with University College London, UK
[54] also at University of Hamburg, Germany
[55] now at Univ. of Wuppertal, Germany
[56] now at DESY group FEB, Hamburg, Germany
[57] also at Institut of Theoretical and Experimental Physics, Moscow, Russia
[58] also at INP, Cracow, Poland
[59] now at ICEPP, University of Tokyo, Japan
[60] also at University of Tokyo, Japan
[61] now at CERN, Geneva, Switzerland
[62] also at Max Planck Institute, Munich, Germany
[63] Department of Radiological Science, Tokyo Institute of Technology, Tokyo, Japan
[64] also at Łódź University, Poland
[65] Łódź University, Poland
[66] also affiliated with DESY

Received: 4 December 2006 / Revised version: 23 January 2007 /
Published online: 20 February 2007 –

Abstract. The photoproduction of dijet events, where the two jets with the highest transverse energy are separated by a large gap in pseudorapidity, have been studied with the ZEUS detector using an integrated luminosity of 39 pb^{-1}. Rapidity-gap events are defined in terms of the energy flow between the jets, such that the total summed transverse energy in this region is less than some value $E_{\mathrm{T}}^{\mathrm{CUT}}$. The data show a clear excess over the predictions of standard photoproduction models. This is interpreted as evidence for a strongly interacting exchange of a color-singlet object. Monte Carlo models which include such a color-singlet exchange are able to describe the data.

[a] supported by DESY, Germany
[b] deceased
[c] Alexander von Humboldt Fellow
[d] self-employed
[e] retired
[f] formerly U. Meyer
[g] supported by Chonnam National University in 2005
[h] supported by a scholarship of the World Laboratory Björn Wiik Research Project
[i] supported by the research grant no. 1 P03B 04529 (2005–2008)
[j] on leave of absence from FPACS, AGH-UST, Cracow, Poland
[k] e-mail: gallo@mail.desy.de
[l] partly supported by Moscow State University, Russia
[m] Ramón y Cajal Fellow
[n] partly supported by Russian Foundation for Basic Research grant no. 05-02-39028-NSFC-a
[o] EU Marie Curie Fellow
[p] partially supported by Warsaw University, Poland
[q] Alexander von Humboldt Research Award supported by DESY, Germany
[r] now at KEK, Tsukuba, Japan
[s] PPARC Advanced fellow
[t] supported by the Polish Ministry for Education and Science grant no. 1 P03B 12629
[u] supported by the Polish Ministry for Education and Science grant no. 1 P03B 14129
[v] supported by the US Department of Energy
[w] supported by the Italian National Institute for Nuclear Physics (INFN)
[x] supported by the German Federal Ministry for Education and Research (BMBF), under contract numbers HZ1GUA 2, HZ1GUB 0, HZ1PDA 5, HZ1VFA 5
[y] supported by the Particle Physics and Astronomy Research Council, UK
[z] supported by the Korean Ministry of Education and Korea Science and Engineering Foundation
[aa] supported by the Malaysian Ministry of Science, Technology and Innovation/Akademi Sains Malaysia grant SAGA 66-02-03-0048
[ab] supported by the US National Science Foundation
[ac] supported by the Polish State Committee for Scientific Research, grant no. 620/E-77/SPB/DESY/P-03/DZ 117/2003-2005 and grant no. 1P03B07427/2004-2006
[ad] supported by the Polish Ministry of Scientific Research and Information Technology, grant no. 112/E-356/SPUB/DESY/P-03/DZ 116/2003-2005 and 1 P03B 065 27
[ae] supported by FNRS and its associated funds (IISN and FRIA) and by an Inter-University Attraction Poles Programme subsidised by the Belgian Federal Science Policy Office
[af] supported by the Spanish Ministry of Education and Science through funds provided by CICYT
[ag] supported by the Natural Sciences and Engineering Research Council of Canada (NSERC)
[ah] partially supported by the German Federal Ministry for Education and Research (BMBF)
[ai] supported by RF Presidential grant N 1685.2003.2 for the leading scientific schools and by the Russian Ministry of Education and Science through its grant for Scientific Research on High Energy Physics
[aj] supported by the Netherlands Foundation for Research on Matter (FOM)
[ak] supported by the German-Israeli Foundation and the Israel Science Foundation
[al] supported by the Japanese Ministry of Education, Culture, Sports, Science and Technology (MEXT) and its grants for Scientific Research
[am] supported in part by the MINERVA Gesellschaft für Forschung GmbH, the Israel Science Foundation (grant no. 293/02-11.2) and the U.S.-Israel Binational Science Foundation

1 Introduction

The production of events in hadronic collisions with two high transverse energy jets in the final state separated by a large rapidity interval provides an ideal environment to study the interplay between soft (non-perturbative) and hard (perturbative) QCD.

The dominant mechanism for the production of jets with high transverse energy in hadronic collisions is a hard interaction between partons in the incoming hadrons via a quark or gluon propagator. The exchange of color quantum numbers generally gives rise to jets in the final state that are color connected to each other and to the remnants of the incoming hadrons. This leads to energy flow populating the pseudorapidity[1] region both between the jets and the hadronic remnants, and between the jets themselves. The fraction of events with little or no hadronic activity between the jets is expected to be exponentially suppressed as the rapidity interval between the jets increases. A non-exponentially suppressed fraction of such events would therefore be a signature of the exchange of a color-singlet (CS) object.

The high transverse energy of the jets provides a perturbative hard scale at each end of the CS exchange, so

[1] The pseudorapidity $\eta = -\ln[\tan(\theta/2)]$, where θ is a polar angle.

that the cross section should be calculable in perturbative QCD [1].

Previous studies of jets with rapidity gaps have been made in $p\bar{p}$ collisions at the Tevatron [2–7] and in photoproduction at HERA [8, 9], where a quasi-real photon from the incoming positron interacts with the proton. Comparison with different Monte Carlo (MC) models suggested that some contribution of a strong CS exchange is required to describe the data, although the uncertainty on the contribution from standard QCD processes was large.

In the analysis presented in this paper, photoproduction of dijet events with a large rapidity gap between jets is used to investigate the dynamics of color-singlet exchange. The results are based on a larger data sample, than in the previous publications [8, 9]. The MC models were tuned to better describe the data sample at the detector level. The CS contribution is studied and compared to MC models as a function of several kinematic variables and to a recent QCD-resummed calculation [10–12].

2 Experimental set-up

The results presented in this paper correspond to $38.6 \pm 1.6\,\mathrm{pb}^{-1}$ of data taken with the ZEUS detector during the 1996–1997 HERA running period. Positrons of 27.5 GeV collided with protons of 820 GeV, giving a center-of-mass energy of $\sqrt{s} = 300\,\mathrm{GeV}$.

A detailed description of the ZEUS detector can be found elsewhere [13, 14]. A brief outline of the components that are most relevant for this analysis is given below.

Charged particles are measured in the central tracking detector (CTD) [15–17], which operates in a magnetic field of 1.43 T provided by a thin super-conducting solenoid. The CTD consists of 72 cylindrical drift chamber layers, organized in nine super-layers covering the polar-angle[2] region $15^\circ < \theta < 164^\circ$. The transverse momentum resolution for full-length tracks can be parameterized as $\sigma(p_\mathrm{T})/p_\mathrm{T} = 0.0058 p_\mathrm{T} \oplus 0.0065 \oplus 0.0014/p_\mathrm{T}$, with p_T in GeV. The tracking system was used to measure the interaction vertex with a typical resolution along (transverse to) the beam direction of 0.4 (0.1) cm and also to cross-check the energy scale of the calorimeter.

The high-resolution uranium-scintillator calorimeter (CAL) [18–21] covers 99.7% of the total solid angle and consists of three parts: the forward (FCAL), the barrel (BCAL) and the rear (RCAL) calorimeters. Each part is subdivided transversely into towers and longitudinally into one electromagnetic section and either one (in RCAL) or two (in BCAL and FCAL) hadronic sections. The smallest subdivision of the calorimeter is called a cell. Under test-beam conditions, the CAL single-particle relative energy resolutions were $\sigma(E)/E = 0.18/\sqrt{E}$ for electrons and $\sigma(E)/E = 0.35/\sqrt{E}$ for hadrons, with E in GeV.

The luminosity was measured from the rate of the bremsstrahlung process $ep \to e\gamma p$. The resulting small angle energetic photons were measured by the luminosity monitor [22–24], a lead-scintillator calorimeter placed in the HERA tunnel at $Z = -107$ m.

3 Kinematics and event selection

A three-level trigger system was used to select events online [14, 25]. In the third-level trigger, jets were required to have a transverse energy of $E_\mathrm{T}^\mathrm{jet} > 4\,\mathrm{GeV}$ and a pseudorapidity of $\eta^\mathrm{jet} < 2.5$ in the laboratory frame.

The γp center-of-mass energy, W, and the inelasticity, $y = W^2/s$, were reconstructed using the Jacquet–Blondel (JB) [26] method. The hadronic system was reconstructed using energy flow objects (EFOs), which were formed by combining information from energy clusters reconstructed in the CAL and charged tracks reconstructed in the CTD. The electron (e) [27] reconstruction method was also used, in order to remove deep inelastic scattering (DIS) events.

The photoproduction sample was selected by applying the following offline cuts:

- the longitudinal position of the reconstructed vertex was required to be in the range $-40\,\mathrm{cm} < Z_\mathrm{VTX} < 40\,\mathrm{cm}$;
- events with a scattered positron in the CAL having $y_e < 0.85$ and $E'_e > 5\,\mathrm{GeV}$, where E'_e is the energy of the scattered positron, were rejected. This cut reduced contamination from neutral current DIS events, since the efficiency for the detection of the scattered positron in this region approached 100%;
- events were required to have $0.2 < y_\mathrm{JB} < 0.75$. The upper cut on y_JB further reduced contamination from the neutral current DIS events that were not removed by the cut on y_e and the lower cut removed beam-gas events;
- in order to reduce contributions from charged current events and cosmic-ray showers, events were required to have a relative transverse momentum $P_\mathrm{T}^\mathrm{miss}/\sqrt{E_\mathrm{T}} < 2.0\,\mathrm{GeV}^{1/2}$, where $P_\mathrm{T}^\mathrm{miss}$ and E_T are the total event missing momentum and transverse energy, respectively.

The cuts on y_e and y_JB reduced the contribution of DIS events to less than 0.5%, confined the phase-space region of the analysis to $0.2 < y < 0.75$ and restricted the photon virtuality to a range of $Q^2 < 1\,\mathrm{GeV}^2$ with a median value of $Q^2 \sim 10^{-3}\,\mathrm{GeV}^2$ [28].

Jets were reconstructed from the EFOs using the k_T algorithm [29] in the longitudinally invariant inclusive mode [30], which implies that any particle is included in one of the jets, and ordered in $E_\mathrm{T}^\mathrm{jet}$, such that jet1 had the highest $E_\mathrm{T}^\mathrm{jet}$. Events in which jets satisfied the following criteria were then selected:

- jet transverse energy corresponding to $E_\mathrm{T}^\mathrm{jet1} \geq 6\,\mathrm{GeV}$ and $E_\mathrm{T}^\mathrm{jet2} \geq 5\,\mathrm{GeV}$ at the hadron level, after taking in

[2] The ZEUS coordinate system is a right-handed Cartesian system, with the Z axis pointing in the proton beam direction, referred to as the "forward direction", and the X axis pointing left towards the center of HERA. The coordinate origin is at the nominal interaction point.

account energy loss in inactive material and other detector effects;
- $-2.4 < \eta^{\mathrm{jet}1,2} < 2.4$, where $\eta^{\mathrm{jet}1}$ and $\eta^{\mathrm{jet}2}$ are the pseudorapidities of the corresponding jets, to ensure that the jets were well reconstructed in the detector;
- $2.5 < \Delta\eta < 4$, where $\Delta\eta \equiv |\eta^{\mathrm{jet}1} - \eta^{\mathrm{jet}2}|$ is the absolute difference in pseudorapidity between the jets;
- $\frac{1}{2}|\left(\eta^{\mathrm{jet}1} + \eta^{\mathrm{jet}2}\right)| < 0.75$, where this condition, together with the previous one, constrained the jets to lie within the kinematic region where the detector and event simulation are well understood.

The transverse energy in the gap, $E_{\mathrm{T}}^{\mathrm{GAP}}$, was calculated by summing up the transverse energy of all jets, without any cut on $E_{\mathrm{T}}^{\mathrm{jet}}$, lying in the pseudorapidity region between the two highest-$E_{\mathrm{T}}^{\mathrm{jet}}$ jets satisfying the above requirements [31]. Gap events were defined as those in which $E_{\mathrm{T}}^{\mathrm{GAP}}$ was less than an $E_{\mathrm{T}}^{\mathrm{CUT}}$ value. The $E_{\mathrm{T}}^{\mathrm{CUT}}$ values used in this analysis were $E_{\mathrm{T}}^{\mathrm{CUT}} = 0.5, 1.0, 1.5,$ and 2.0 GeV. The gap fraction, f, was defined as the ratio of the cross section for gap events to the cross section for inclusive events, which pass all of the above cuts but have no restriction on the $E_{\mathrm{T}}^{\mathrm{GAP}}$ value.

In addition, the fraction of the photon momentum participating in the hard interaction was calculated as $x_\gamma^{\mathrm{OBS}} = (E_{\mathrm{T}}^{\mathrm{jet}1} e^{-\eta^{\mathrm{jet}1}} + E_{\mathrm{T}}^{\mathrm{jet}2} e^{-\eta^{\mathrm{jet}2}})/2yE_e$, where E_e is the energy of the positron beam.

4 QCD models and event simulation

4.1 Monte Carlo models

The *Pythia 6.1* [32] and *Herwig 6.1* [33] MC generators were used to correct the data to the hadron level and for model comparisons. Both MCs are based on the leading order (LO) $(2 \to 2)$ matrix elements together with a parton-shower simulation of additional QCD radiation and hadronisation models. The detector simulation was performed with the *Geant* 3.13 program [34].

In photoproduction interactions at LO, the photon can either participate directly in the hard sub-process (direct photoproduction) or first fluctuate into a hadronic state which then interacts via a partonic constituent carrying some fraction, x_γ, of the photon momentum (resolved photoproduction). At leading order, therefore, CS exchange between jets may take place only in resolved photoproduction. For this analysis the direct, resolved, and CS exchange MC samples were generated separately.

The simulation of multi-parton interactions (MPI) was included in *Pythia* using the so-called "simple mode" [32] and in *Herwig* by interfacing to the *Jimmy* library [35]. The minimum transverse momenta, $p_{\mathrm{T}}^{\mathrm{min}}$, of the outgoing partons in the hard interaction and partons participating in MPI are separately adjustable in *Pythia*, while in *Herwig* the same parameter was used to adjust both momenta. The starting parameters for the tuning were taken from global fits of *JetWeb* [36]. The $p_{\mathrm{T}}^{\mathrm{min}}$ was tuned [37, 38] for both MC programs by comparing to the data sample after the kinematic cuts were applied (see Sect. 3). The best fit resulted in $p_{\mathrm{T}}^{\mathrm{min}}$ values of $p_{\mathrm{T}}^{\mathrm{min1}} = 1.9$ GeV and $p_{\mathrm{T}}^{\mathrm{min2}} = 1.7$ GeV for *Pythia* and $p_{\mathrm{T}}^{\mathrm{min}} = 2.7$ GeV for *Herwig*. For both MC models the CTEQ5L parametrisation [39] for the proton and the SaS-G 2D parametrisation [40] for the photon PDFs were used. Hadronisation in *Herwig* is simulated using the cluster model [41] while *Pythia* uses the Lund string model [42].

The CS exchange is implemented in *Herwig* using the LLA BFKL model by Mueller and Tang [43]. The hard-Pomeron intercept, $1 + \omega_0$, is related to the strong coupling, α_s, used in the BFKL parton evolution by $\omega_0 = \frac{\alpha_s C_{\mathrm{A}}}{\pi}\,[4\ln(2)]$. In this analysis, the default value of $\omega_0 = 0.3$ was used.

Pythia does not contain a simulation of strongly interacting CS exchange in hard interactions. However, a similar topology can be simulated by high-t photon exchange for quark–quark scattering in LO resolved processes. Such an exchange is not expected to represent the mechanism of strongly-interacting CS exchange and is only used to compare the data to an alternative CS model.

4.2 Resummed calculation

The gap definition in terms of the energy flow between jets, being infrared safe, allows pQCD calculations to be applied. These calculations involve the resummation of large logarithms of $E_{\mathrm{T}}^{\mathrm{GAP}}/E_{\mathrm{T}}^{\mathrm{jet}}$. There are several sources of these large logarithms. The primary leading logarithms arise from soft gluon emission directly into the gap, whereas secondary (non-global) leading logarithms are due to emission into the gap from a coherent ensemble of gluons outside the gap region [11, 12, 44–49].

The calculation [10] used in this paper provides a prediction of the gap fraction with primary emission resummed to all orders and a correction applied for the effect of the clustering algorithm, and the non-global logarithms correct in the limit of large number of colors. The theoretical uncertainty in this calculation is estimated from varying the renormalisation scale between $E_{\mathrm{T}}/2$ and $2E_{\mathrm{T}}$, where E_{T} is the transverse energy of the hardest jet.

5 Data correction and systematic uncertainties

The data were corrected to the hadron level, bin-by-bin, using correction factors obtained from a combination of direct, resolved, and CS MC samples as described in detail elsewhere [37, 38].

The admixture of direct and resolved MC used in the unfolding was determined by the best fit to the x_γ^{OBS} data distribution. The combination of direct and resolved MC formed the non-color-singlet (NCS) sample.

The relative amounts of NCS and CS MC used in the unfolding were determined by the best fit to the total energy in the gap for events in which $E_{\mathrm{T}}^{\mathrm{GAP}} < 1.5$ GeV, after the normalisation of the NCS sample was fixed using data

at $E_{\mathrm{T}}^{\mathrm{GAP}} > 1.5\,\mathrm{GeV}$. Fitting to the total number of jets in the gap for events in which $E_{\mathrm{T}}^{\mathrm{GAP}} < 1.5\,\mathrm{GeV}$ and to $\mathrm{d}\sigma/\mathrm{d}E_{\mathrm{T}}^{\mathrm{GAP}}$ gave similar results.

To correct the data the average correction factor of *Pythia* and *Herwig* was used. One half of the difference between those two models predictions, about 5%, was assigned to the systematic uncertainties.

A detailed study of the sources contributing to the systematic uncertainties of the measurements was performed using *Herwig*. The analysis cuts were varied by their respective resolutions estimated using Monte Carlo.

The variation of the cuts on $E_{\mathrm{T}}^{\mathrm{GAP}}$ and E_{T} caused the largest contributions to the systematic uncertainty. Depending upon the variable measured, their contribution ranged from a few to approximately 30% in regions where the statistical significance was low.

The amount of CS exchange MC used in the unfolding was varied by ±25%, resulting in a variation in the cross section at the one percent level. All the above systematics were added in quadrature in order to calculate the total systematic uncertainty.

The calorimeter energy scale was varied by ±3%. This uncertainty was not combined with the other systematics, but instead shown separately as a shaded band in the figures.

6 Results

The inclusive dijet cross section as a function of $E_{\mathrm{T}}^{\mathrm{GAP}}$ is presented in Fig. 1 and Table 1. At low $E_{\mathrm{T}}^{\mathrm{GAP}}$ values, where the CS contribution should be most pronounced, the data demonstrate a clear excess over the NCS MC predictions. In order to estimate the amount of CS contribution, the direct and resolved components of each MC were mixed according to their predicted MC cross sections to give the NCS MC sample. The NCS and CS MC samples were then fitted to the data according to

$$\frac{\mathrm{d}\sigma}{\mathrm{d}E_{\mathrm{T}}^{\mathrm{GAP}}} = P_1 \frac{\mathrm{d}\sigma^{\mathrm{NCS}}}{\mathrm{d}E_{\mathrm{T}}^{\mathrm{GAP}}} + P_2 \frac{\mathrm{d}\sigma^{\mathrm{CS}}}{\mathrm{d}E_{\mathrm{T}}^{\mathrm{GAP}}},$$

Table 1. The measured differential cross section $\mathrm{d}\sigma/\mathrm{d}E_{\mathrm{T}}^{\mathrm{GAP}}$ unfolded with the average correction factors of *Pythia* and *Herwig* for the inclusive sample of events. The statistical error, systematic errors, and calorimeter energy-scale uncertainty on the measurement are also listed

$E_{\mathrm{T}}^{\mathrm{GAP}}$ bin (GeV)	σ(nb/GeV)	± stat	± sys	± cal
0.0 – 0.5	0.167	±0.004	$^{+0.014}_{-0.014}$	$^{+0.002}_{-0.006}$
0.5 – 1.5	0.153	±0.002	$^{+0.006}_{-0.006}$	$^{+0.000}_{-0.001}$
1.5 – 3.5	0.210	±0.002	$^{+0.009}_{-0.008}$	$^{+0.001}_{-0.002}$
3.5 – 7.0	0.177	±0.001	$^{+0.006}_{-0.005}$	$^{+0.006}_{-0.008}$
7.0 – 12.0	0.080	±0.001	$^{+0.002}_{-0.002}$	$^{+0.007}_{-0.008}$

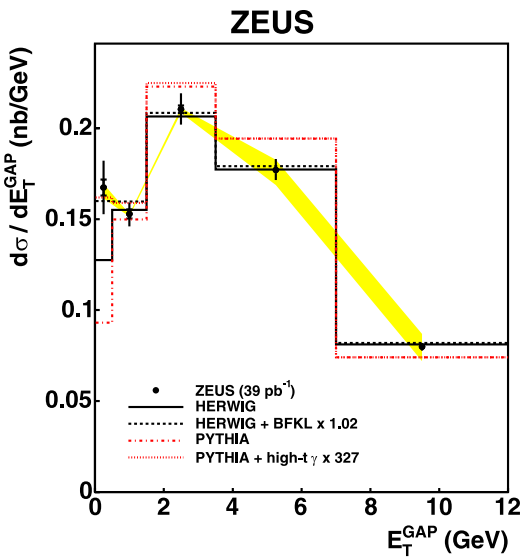

Fig. 1. The inclusive dijet cross section, differential in $E_{\mathrm{T}}^{\mathrm{GAP}}$. The *black circles* represent the ZEUS data, with the *inner error bars* representing the statistical errors and the *outer error bars* representing the statistical and systematic uncertainties added in quadrature. The *solid black line* shows the prediction of *Herwig* and the *black dashed line* shows the prediction of *Herwig* plus *BFKL* Pomeron exchange. The *dot-dashed line* shows the prediction of *Pythia* and *the dotted line* shows the prediction of *Pythia* plus high-t photon exchange. The *band* shows the calorimeter energy-scale uncertainty

where P_1 and P_2 were the free parameters of the fit. The best fit to the data resulted in $P_1 = 1.31 \pm 0.01$ and $P_2 = 327 \pm 20$ for *Pythia* and $P_1 = 1.93 \pm 0.01$ and $P_2 = 1.02 \pm 0.13$ for *Herwig*. These scaling parameters were used in this analysis when comparing the data to the MC predictions. The large value of P_2 for *Pythia* reflects the very low cross section of the high-t photon exchange, which is not expected to represent the mechanism of strongly-interacting CS exchange. The color-singlet contribution to the total cross section, estimated by integrating the MC predictions over the entire $E_{\mathrm{T}}^{\mathrm{GAP}}$ range, was $(2.75 \pm 0.10)\%$ for *Pythia* and $(2.04 \pm 0.25)\%$ for *Herwig*, where the errors represent only the statistical uncertainties of the fit.

The inclusive dijet cross section, the gap cross section, and the gap fraction as a function of the separation of the two leading jets, $\Delta\eta$, are presented in Fig. 2 for $E_{\mathrm{T}}^{\mathrm{CUT}} = 1\,\mathrm{GeV}$. Both cross sections and gap fractions decrease as a function of $\Delta\eta$. In the inclusive cross section, both MC models with and without CS exchange describe the data equally well. For the gap cross section the MC models without CS exchange fall below the data, while the MC models with CS exchange agree with the data. The contribution of CS exchange to the total gap fraction increases as the dijet separation increases from 2.5 to 4 units in pseudorapidity.

Figure 3 shows the gap fraction as a function of $\Delta\eta$ for the four values of $E_{\mathrm{T}}^{\mathrm{CUT}} = 0.5, 1.0, 1.5$ and $2\,\mathrm{GeV}$. The corresponding values are listed in Table 2. The data

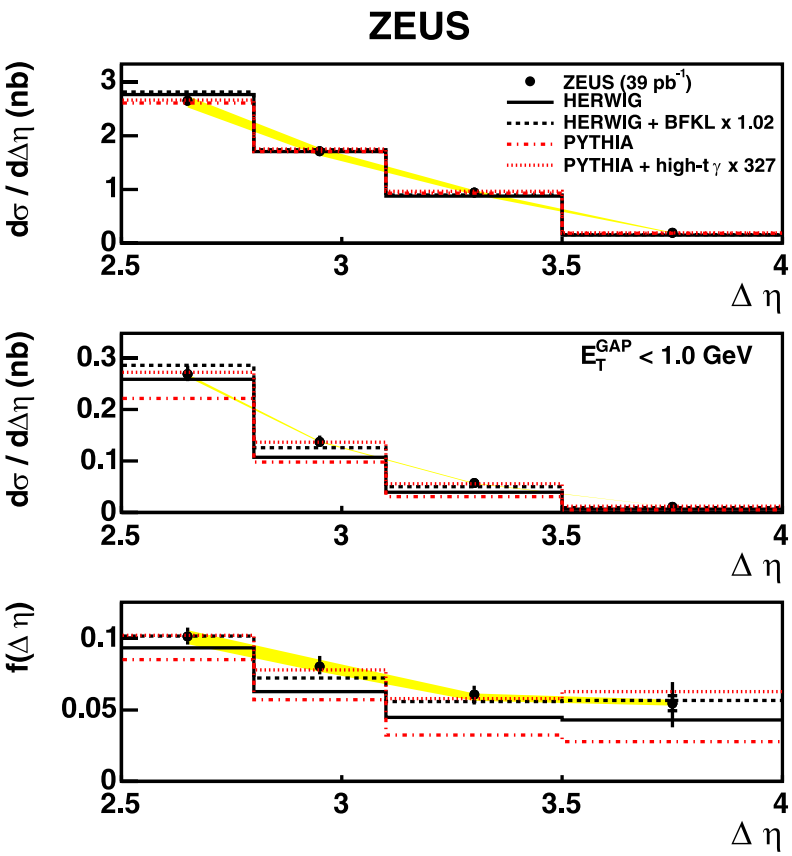

Fig. 2. The *top plot* is the inclusive dijet cross section differential in $\Delta\eta$, the *middle plot* is the gap cross section differential in $\Delta\eta$ requiring that $E_{\mathrm{T}}^{\mathrm{GAP}} < 1\,\mathrm{GeV}$, and the *bottom plot* is the gap fraction, f, as a function of $\Delta\eta$. Other details as in Fig. 1

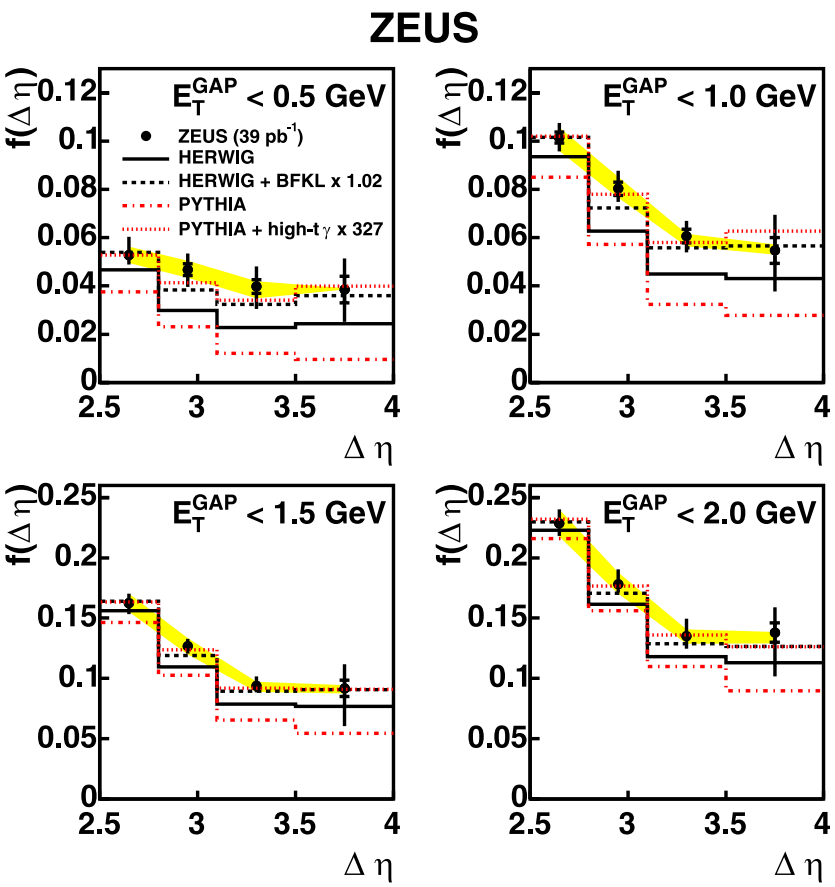

Fig. 3. The gap fraction, f, as a function of $\Delta\eta$ for different requirements on $E_{\mathrm{T}}^{\mathrm{GAP}}$. Other details as in Fig. 1

Table 2. The measured gap fraction $f(\Delta\eta)$ unfolded with the average correction factors of *Pythia* and *Herwig*. The statistical error, systematic errors, and calorimeter energy-scale uncertainty on the measurement are also listed

$\Delta\eta$ bin	E_T^{CUT} GeV	f	$\pm$ stat	$\pm$ sys	$\pm$ cal
2.5, 2.8	0.5	0.053	$\pm$ 0.002	$^{+0.007}_{-0.004}$	$^{+0.003}_{-0.003}$
2.8, 3.1		0.047	$\pm$ 0.002	$^{+0.006}_{-0.007}$	$^{+0.004}_{-0.003}$
3.1, 3.5		0.040	$\pm$ 0.003	$^{+0.008}_{-0.009}$	$^{+0.002}_{-0.005}$
3.5, 4.0		0.038	$\pm$ 0.005	$^{+0.012}_{-0.012}$	$^{+0.001}_{-0.000}$
2.5, 2.8	1.0	0.101	$\pm$ 0.002	$^{+0.006}_{-0.005}$	$^{+0.004}_{-0.005}$
2.8, 3.1		0.080	$\pm$ 0.003	$^{+0.007}_{-0.005}$	$^{+0.005}_{-0.004}$
3.1, 3.5		0.061	$\pm$ 0.003	$^{+0.006}_{-0.006}$	$^{+0.001}_{-0.004}$
3.5, 4.0		0.055	$\pm$ 0.005	$^{+0.014}_{-0.016}$	$^{+0.003}_{-0.002}$
2.5, 2.8	1.5	0.163	$\pm$ 0.003	$^{+0.007}_{-0.009}$	$^{+0.008}_{-0.007}$
2.8, 3.1		0.127	$\pm$ 0.003	$^{+0.005}_{-0.005}$	$^{+0.007}_{-0.007}$
3.1, 3.5		0.094	$\pm$ 0.003	$^{+0.007}_{-0.005}$	$^{+0.003}_{-0.005}$
3.5, 4.0		0.092	$\pm$ 0.007	$^{+0.019}_{-0.030}$	$^{+0.003}_{-0.004}$
2.5, 2.8	2.0	0.228	$\pm$ 0.003	$^{+0.011}_{-0.010}$	$^{+0.012}_{-0.011}$
2.8, 3.1		0.178	$\pm$ 0.004	$^{+0.012}_{-0.006}$	$^{+0.010}_{-0.008}$
3.1, 3.5		0.135	$\pm$ 0.004	$^{+0.014}_{-0.010}$	$^{+0.006}_{-0.006}$
3.5, 4.0		0.138	$\pm$ 0.008	$^{+0.019}_{-0.035}$	$^{+0.001}_{-0.009}$

first fall and then level out as $\Delta\eta$ increases for all values of E_T^{CUT}, although for $E_T^{CUT} = 0.5$ the data are consistent with a flat distribution in $\Delta\eta$. The predictions of *Pythia* and *Herwig* without CS exchange lie below the data over the entire $\Delta\eta$ range. With the addition of the CS contribution, both MC models describe the data well.

The previously published ZEUS results [8] used a different definition of the rapidity gap and so cannot be directly compared. The present results agree with the previous H1 measurement [9], where the gap definition used the transverse energy in the gap as for the current analysis, but with slightly different kinematic cuts. The comparison is shown in Fig. 4, where the H1 data have been scaled bin-by-bin with multiplicative factors estimated using the *Herwig* MC predictions for the gap fractions at the hadron level to account for the difference in the phase space between the ZEUS and H1 analyses.

Figure 5 shows the gap fraction for four different values of E_T^{CUT} compared to the resummed calculation [10]. The shape of the data as a function of $\Delta\eta$ is reasonably well described for all values of E_T^{CUT} but the predictions lie above the data, almost everywhere outside of the range defined by the theoretical uncertainties.

For comparison with other experiments and $p\bar{p}$ measurements, which are expected to be similar to the resolved-photon process, the cross sections and gap fraction were also measured as function of x_γ^{OBS}. These results are pre-

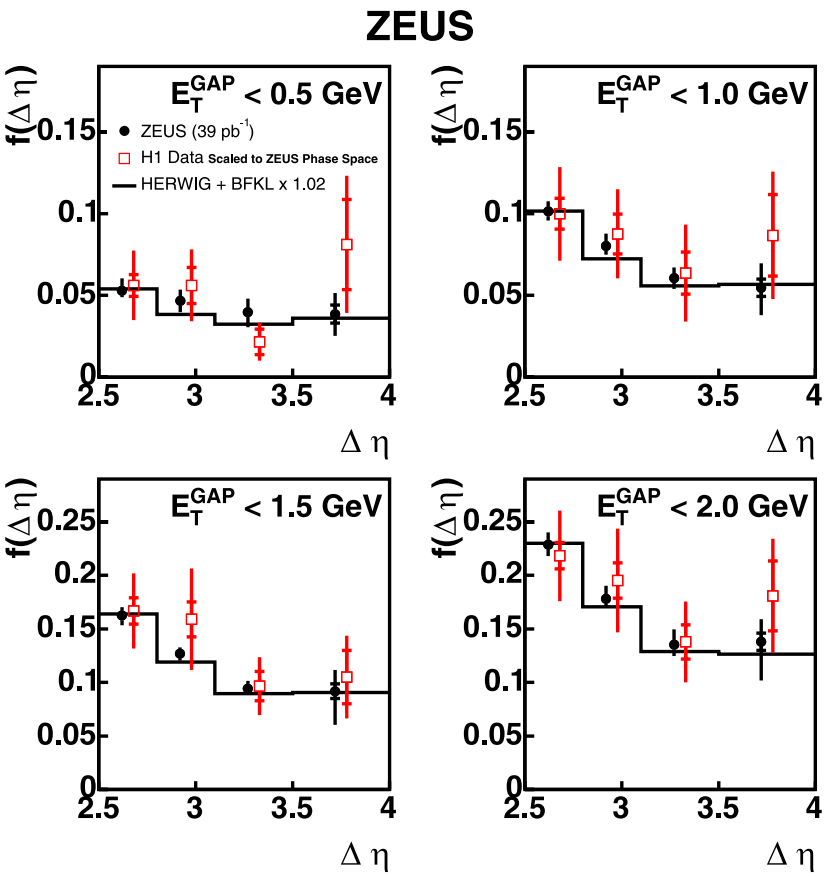

Fig. 4. The gap fraction, f, as a function of $\Delta\eta$ for different requirements on E_T^{GAP}. The *black circles* represent the ZEUS data, with the *inner error bars* representing the statistical errors and the *outer error bars* representing the statistical and systematic uncertainties added in quadrature. The *solid black line* shows the prediction of *Herwig* plus *BFKL* Pomeron exchange. The *open squares* represent the H1 data [9] scaled for comparison to the ZEUS phase space as described in the text

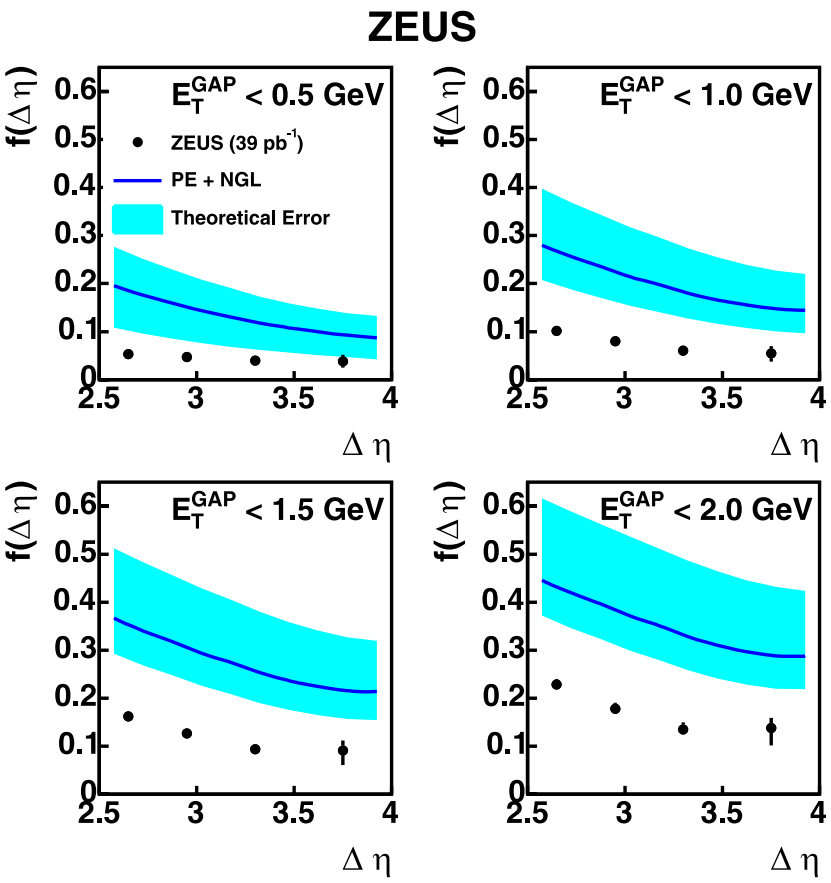

Fig. 5. The gap fraction, f, as a function of $\Delta\eta$ for different requirements on $E_{\mathrm{T}}^{\mathrm{GAP}}$. The *black circles* represent the ZEUS data, with *the error bars* representing the statistical and systematic uncertainties added in quadrature. The resummed calculation [10] is shown by *the solid curve* and the renormalization scale uncertainty is shown by *the shaded band*. The data are plotted at the 4 bin centers in $\Delta\eta$ and the theory curve was produced by joining the bin centers for the ratios of the integrated cross sections for 8 bins in $\Delta\eta$

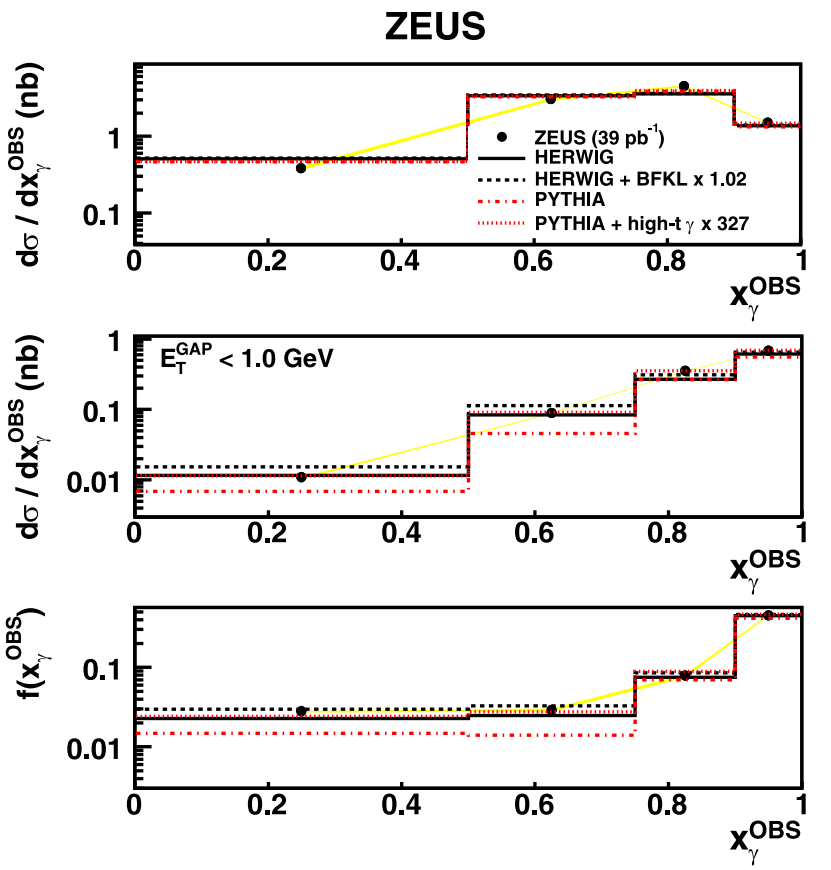

Fig. 6. The *top plot* is the inclusive dijet cross section differential in x_γ^{OBS}, the *middle plot* is the gap cross section differential in x_γ^{OBS} requiring that $E_{\mathrm{T}}^{\mathrm{GAP}} < 1\,\mathrm{GeV}$, and the *bottom plot* is the gap fraction, f, as a function of x_γ^{OBS}. Other details as in Fig. 1

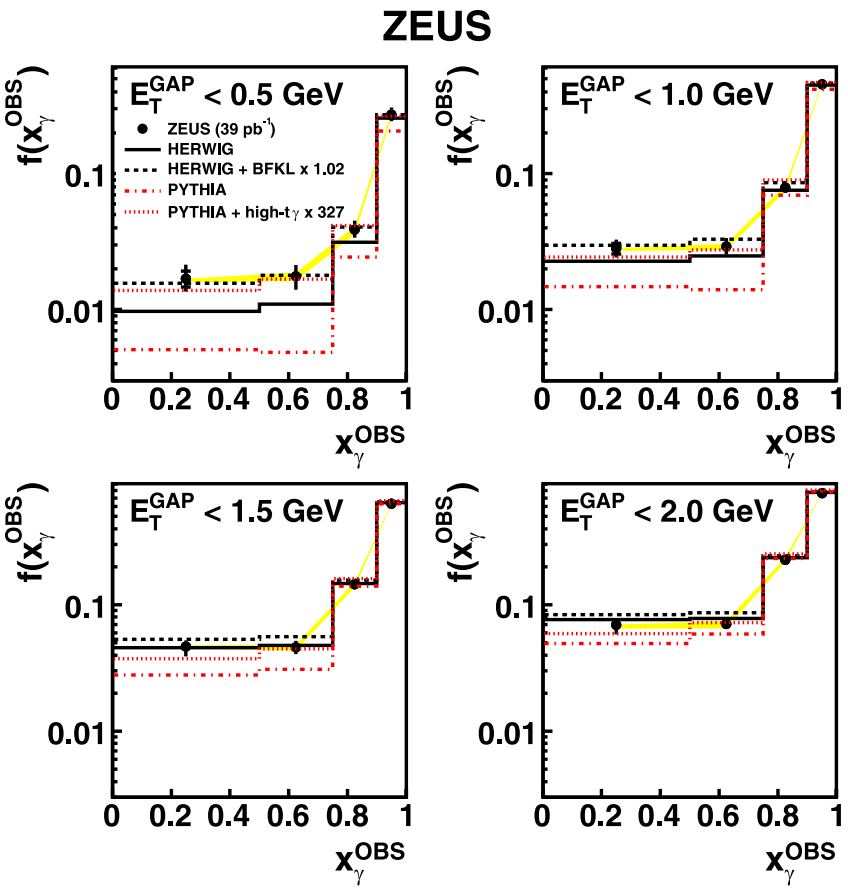

Fig. 7. The gap fraction, f, as a function of $x_\gamma^{\rm OBS}$ for different requirements on $E_{\rm T}^{\rm GAP}$. Other details as in Fig. 1

Table 3. The measured gap fraction f($x_\gamma^{\rm OBS}$) unfolded with the average correction factors of *Pythia* and *Herwig*. The statistical error, systematic errors, and calorimeter energy-scale uncertainty on the measurement are also listed

$x_\gamma^{\rm OBS}$ bin	$E_{\rm T}^{\rm CUT}$ GeV	f	± stat	± sys	± cal
0.00, 0.50	0.5	0.017	± 0.002	$^{+0.004}_{-0.002}$	$^{+0.000}_{-0.001}$
0.50, 0.75		0.018	± 0.001	$^{+0.004}_{-0.003}$	$^{+0.001}_{-0.001}$
0.75, 0.90		0.039	± 0.002	$^{+0.006}_{-0.005}$	$^{+0.002}_{-0.003}$
0.90, 1.00		0.272	± 0.010	$^{+0.033}_{-0.028}$	$^{+0.011}_{-0.012}$
0.00, 0.50	1.0	0.028	± 0.003	$^{+0.004}_{-0.003}$	$^{+0.000}_{-0.001}$
0.50, 0.75		0.029	± 0.001	$^{+0.004}_{-0.003}$	$^{+0.001}_{-0.002}$
0.75, 0.90		0.079	± 0.002	$^{+0.005}_{-0.005}$	$^{+0.003}_{-0.005}$
0.90, 1.00		0.454	± 0.012	$^{+0.024}_{-0.026}$	$^{+0.008}_{-0.008}$
0.00, 0.50	1.5	0.047	± 0.003	$^{+0.005}_{-0.007}$	$^{+0.001}_{-0.002}$
0.50, 0.75		0.046	± 0.001	$^{+0.006}_{-0.005}$	$^{+0.003}_{-0.003}$
0.75, 0.90		0.145	± 0.003	$^{+0.007}_{-0.010}$	$^{+0.006}_{-0.008}$
0.90, 1.00		0.630	± 0.015	$^{+0.028}_{-0.022}$	$^{+0.010}_{-0.007}$
0.00, 0.50	2.0	0.069	± 0.004	$^{+0.007}_{-0.010}$	$^{+0.001}_{-0.005}$
0.50, 0.75		0.070	± 0.002	$^{+0.008}_{-0.005}$	$^{+0.004}_{-0.005}$
0.75, 0.90		0.227	± 0.004	$^{+0.016}_{-0.013}$	$^{+0.010}_{-0.009}$
0.90, 1.00		0.763	± 0.018	$^{+0.023}_{-0.021}$	$^{+0.009}_{-0.003}$

Table 4. The measured gap fraction $f\,(W)$ unfolded with the average correction factors of *Pythia* and *Herwig*. The statistical error, systematic errors, and calorimeter energy-scale uncertainty on the measurement are also listed

W bin (GeV)	$E_{\rm T}^{\rm CUT}$ GeV	f	± stat	± sys	± cal
150.0, 180.0	0.5	0.077	± 0.007	$^{+0.017}_{-0.017}$	$^{+0.001}_{-0.010}$
180.0, 210.0		0.049	± 0.003	$^{+0.008}_{-0.005}$	$^{+0.002}_{-0.001}$
210.0, 240.0		0.039	± 0.002	$^{+0.006}_{-0.005}$	$^{+0.002}_{-0.002}$
240.0, 260.0		0.038	± 0.002	$^{+0.005}_{-0.004}$	$^{+0.003}_{-0.002}$
150.0, 180.0	1.0	0.145	± 0.008	$^{+0.016}_{-0.019}$	$^{+0.003}_{-0.014}$
180.0, 210.0		0.096	± 0.004	$^{+0.005}_{-0.007}$	$^{+0.004}_{-0.001}$
210.0, 240.0		0.069	± 0.002	$^{+0.007}_{-0.004}$	$^{+0.001}_{-0.002}$
240.0, 260.0		0.062	± 0.002	$^{+0.006}_{-0.004}$	$^{+0.005}_{-0.003}$
150.0, 180.0	1.5	0.241	± 0.010	$^{+0.025}_{-0.019}$	$^{+0.003}_{-0.015}$
180.0, 210.0		0.153	± 0.004	$^{+0.010}_{-0.010}$	$^{+0.008}_{-0.004}$
210.0, 240.0		0.113	± 0.003	$^{+0.008}_{-0.008}$	$^{+0.006}_{-0.006}$
240.0, 260.0		0.097	± 0.003	$^{+0.006}_{-0.006}$	$^{+0.003}_{-0.005}$
150.0, 180.0	2.0	0.338	± 0.012	$^{+0.029}_{-0.037}$	$^{+0.010}_{-0.015}$
180.0, 210.0		0.218	± 0.005	$^{+0.016}_{-0.019}$	$^{+0.010}_{-0.004}$
210.0, 240.0		0.163	± 0.003	$^{+0.012}_{-0.011}$	$^{+0.007}_{-0.007}$
240.0, 260.0		0.139	± 0.003	$^{+0.011}_{-0.004}$	$^{+0.006}_{-0.008}$

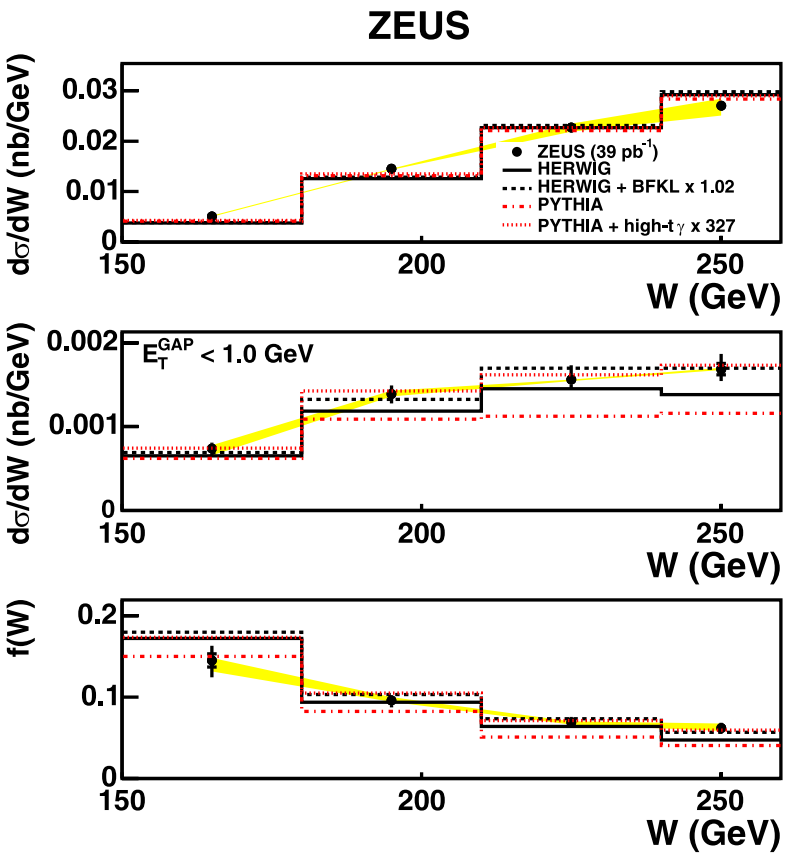

Fig. 8. The *top plot* is the inclusive dijet cross section differential in W, the *middle plot* is the gap cross section differential as a function of W requiring that $E_{\mathrm{T}}^{\mathrm{GAP}} < 1$ GeV, and the *bottom plot* is the gap fraction, f, as a function of W. Other details as in Fig. 1

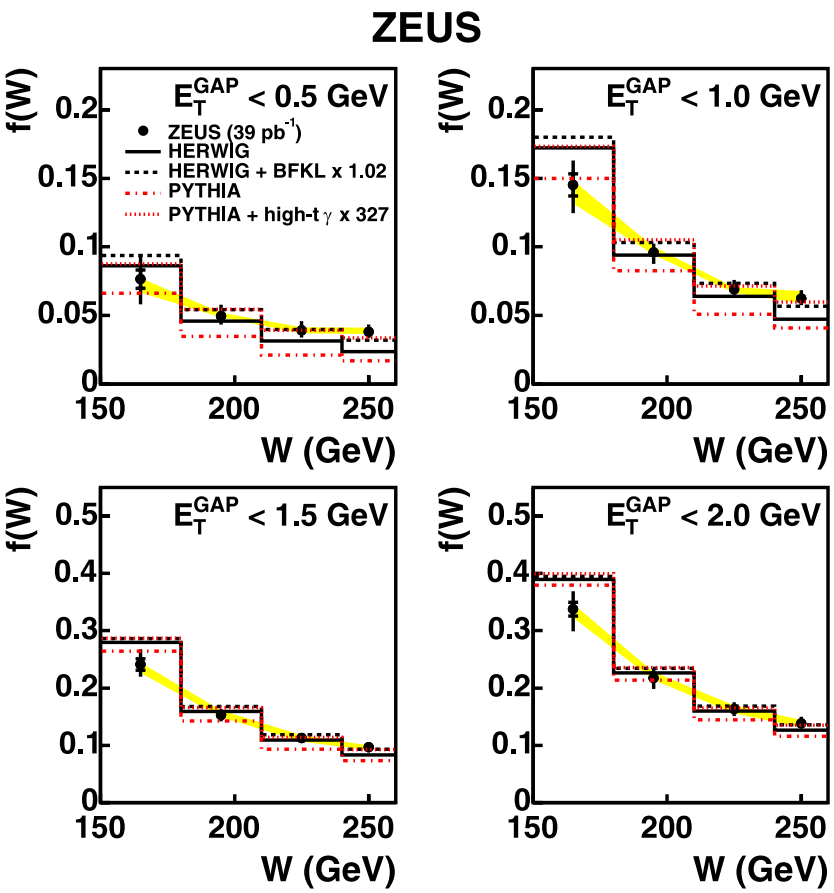

Fig. 9. The gap fraction, f, as a function of W for different requirements on $E_{\mathrm{T}}^{\mathrm{GAP}}$. Other details as in Fig. 1

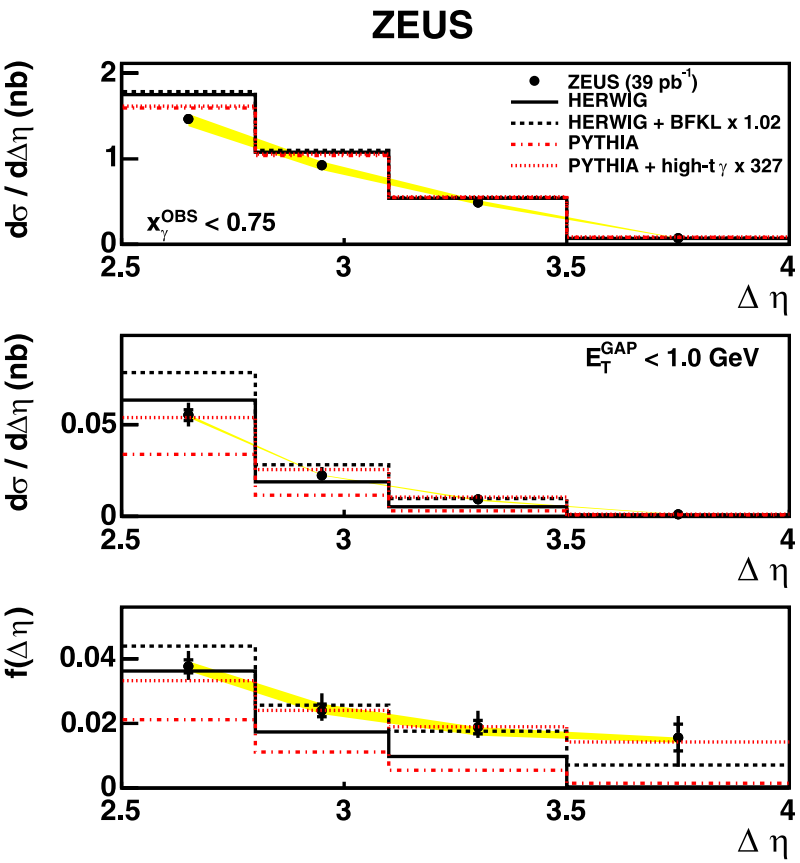

Fig. 10. The *top plot* is the inclusive dijet cross section for $x_\gamma^{\rm OBS} < 0.75$ differential in $\Delta\eta$, the *middle plot* is the corresponding gap cross section differential in $\Delta\eta$ requiring that $E_{\rm T}^{\rm GAP} < 1$ GeV, and the *bottom plot* is the gap fraction, f, as a function of $\Delta\eta$. Other details as in Fig. 1

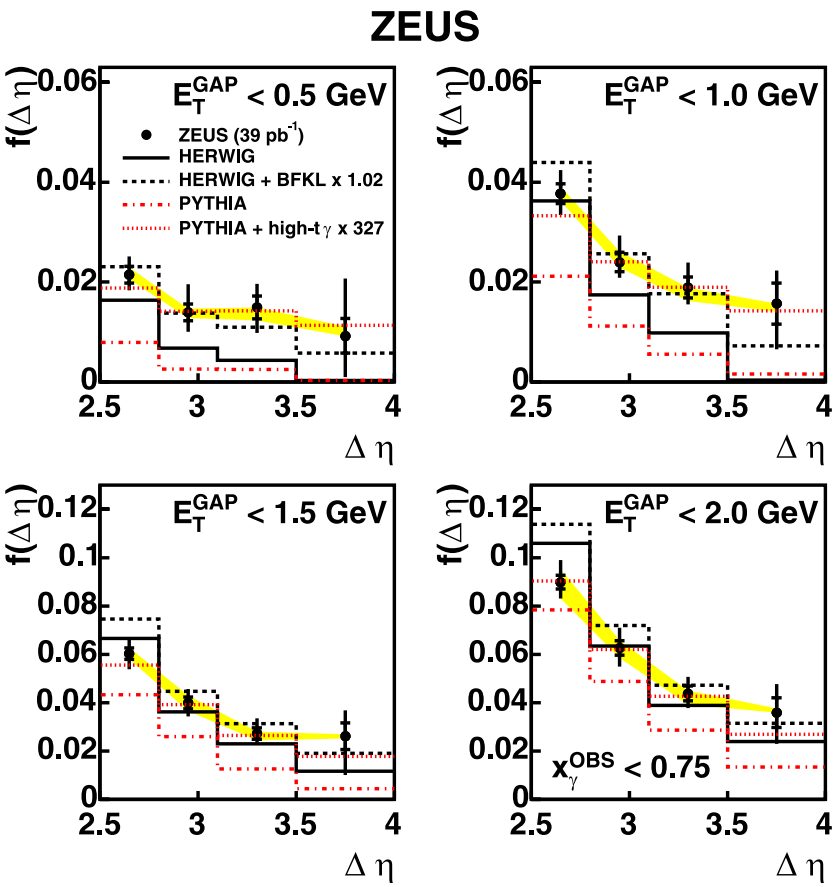

Fig. 11. The gap fraction, f, as a function of $\Delta\eta$ for $x_\gamma^{\rm OBS} < 0.75$ and different requirements on $E_{\rm T}^{\rm GAP}$. Other details as in Fig. 1

Table 5. The measured gap fraction $f(\Delta\eta)$ for the region $x_\gamma^{\rm OBS} < 0.75$ unfolded with the average correction factors of *Pythia* and *Herwig*. The statistical error, systematic errors, and calorimeter energy-scale uncertainty on the measurement are also listed

$\Delta\eta$ bin	$E_{\rm T}^{\rm CUT}$ GeV	f	$\pm$ stat	$\pm$ sys	$\pm$ cal
2.5, 2.8	0.5	0.021	$\pm$ 0.002	$^{+0.003}_{-0.003}$	$^{+0.001}_{-0.001}$
2.8, 3.1		0.014	$\pm$ 0.002	$^{+0.005}_{-0.004}$	$^{+0.001}_{-0.001}$
3.1, 3.5		0.015	$\pm$ 0.002	$^{+0.004}_{-0.005}$	$^{+0.000}_{-0.003}$
3.5, 4.0		0.009	$\pm$ 0.003	$^{+0.011}_{-0.007}$	$^{+0.002}_{-0.000}$
2.5, 2.8	1.0	0.038	$\pm$ 0.002	$^{+0.004}_{-0.004}$	$^{+0.001}_{-0.001}$
2.8, 3.1		0.024	$\pm$ 0.002	$^{+0.005}_{-0.003}$	$^{+0.002}_{-0.001}$
3.1, 3.5		0.019	$\pm$ 0.002	$^{+0.005}_{-0.003}$	$^{+0.000}_{-0.003}$
3.5, 4.0		0.016	$\pm$ 0.004	$^{+0.005}_{-0.008}$	$^{+0.000}_{-0.002}$
2.5, 2.8	1.5	0.060	$\pm$ 0.002	$^{+0.006}_{-0.006}$	$^{+0.003}_{-0.002}$
2.8, 3.1		0.040	$\pm$ 0.002	$^{+0.005}_{-0.005}$	$^{+0.003}_{-0.003}$
3.1, 3.5		0.027	$\pm$ 0.002	$^{+0.006}_{-0.003}$	$^{+0.001}_{-0.003}$
3.5, 4.0		0.026	$\pm$ 0.006	$^{+0.009}_{-0.015}$	$^{+0.001}_{-0.001}$
2.5, 2.8	2.0	0.090	$\pm$ 0.003	$^{+0.009}_{-0.006}$	$^{+0.005}_{-0.007}$
2.8, 3.1		0.063	$\pm$ 0.003	$^{+0.008}_{-0.007}$	$^{+0.003}_{-0.004}$
3.1, 3.5		0.044	$\pm$ 0.003	$^{+0.006}_{-0.005}$	$^{+0.001}_{-0.005}$
3.5, 4.0		0.036	$\pm$ 0.006	$^{+0.010}_{-0.011}$	$^{+0.002}_{-0.000}$

sented in Figs. 6, 7 and Table 3 for four different values of $E_{\rm T}^{\rm CUT}$. The gap fraction decreases with decreasing $x_\gamma^{\rm OBS}$ and the data are reasonably described by both MC models only after including the CS contribution, especially in the resolved-photon region, $x_\gamma^{\rm OBS} < 0.75$, and at low $E_{\rm T}^{\rm GAP}$.

The W dependence, which is important for comparison with experiments at different energies, is presented for the cross sections and gap fractions in Figs. 8, 9 and Table 4. The gap fraction falls with increasing W. Both the cross sections and the gap fractions are described by the MC with CS included.

The $\Delta\eta$ and W dependencies were investigated in the resolved-enhanced region. Figure 10 shows the cross sections as a function of $\Delta\eta$ in the resolved-photon region, $x_\gamma^{\rm OBS} < 0.75$, for $E_{\rm T}^{\rm GAP} < 1$ GeV. The gap fraction as a function of $\Delta\eta$ is reasonably well described by MC models after including the CS contribution. Figure 11 and Table 5 show the gap fractions as a function of $\Delta\eta$ for the resolved-enhanced sample for the four $E_{\rm T}^{\rm CUT}$ values. For $E_{\rm T}^{\rm GAP} < 0.5$ GeV and $E_{\rm T}^{\rm GAP} < 1.0$ GeV, both MC models predict almost no contribution to the gap fractions from the NCS component at high values of $\Delta\eta$. The W behavior in the resolved-enhanced sample is presented in Figs. 12 and 13 and Table 6.

Although the gap fraction was measured with small errors, the difference in the model predictions precludes a model-independent determination of the CS contribution.

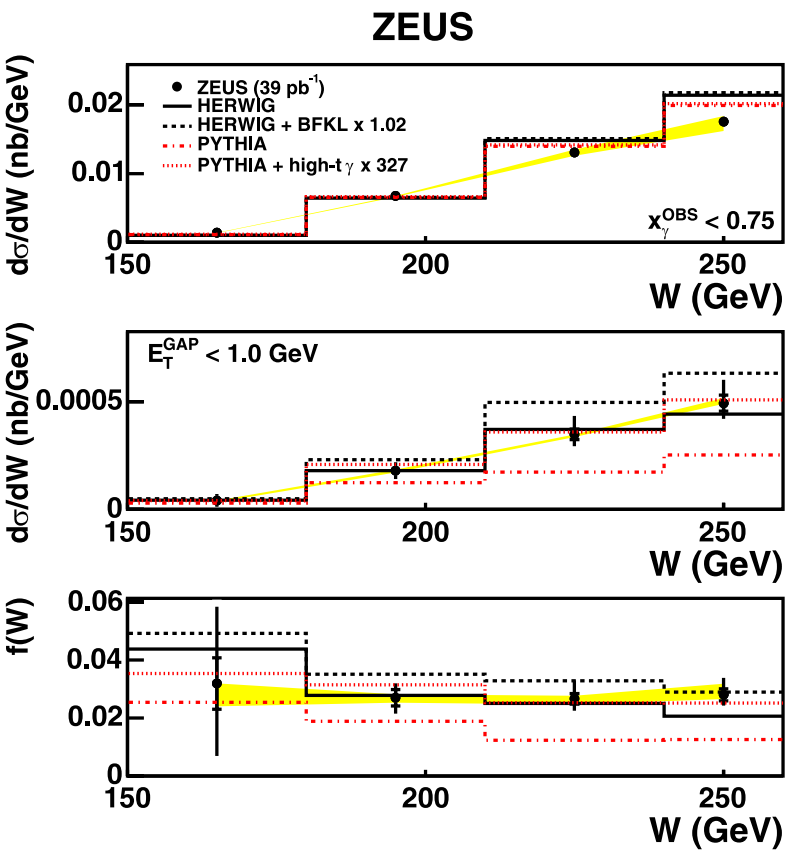

Fig. 12. The *top plot* is the inclusive dijet cross section for $x_\gamma^{\rm OBS} < 0.75$ differential in W, the *middle plot* is the corresponding gap cross section differential in W requiring that $E_{\rm T}^{\rm GAP} < 1$ GeV, and the *bottom plot* is the gap fraction, f, as a function of W. Other details as in Fig. 1

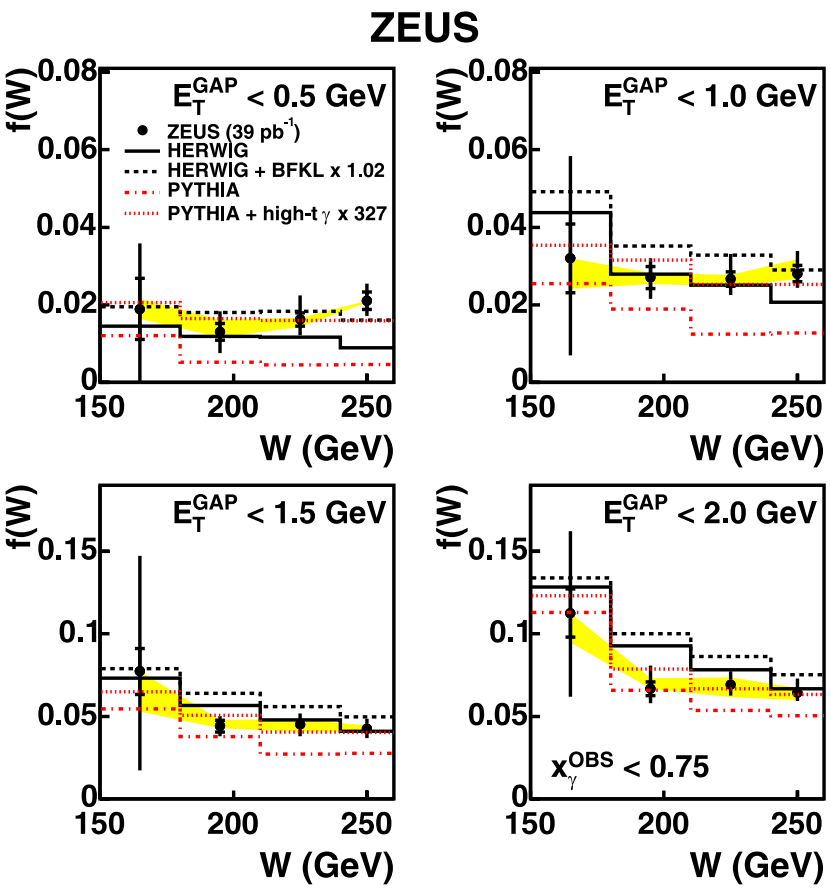

Fig. 13. The gap fraction, f, as a function of W, for $x_\gamma^{\mathrm{OBS}} < 0.75$ and different requirements on $E_{\mathrm{T}}^{\mathrm{GAP}}$. Other details as in Fig. 1

Table 6. The measured gap fraction $f\ (W)$ for the region $x_\gamma^{\mathrm{OBS}} < 0.75$ unfolded with the average correction factors of *Pythia* and *Herwig*. The statistical error, systematic errors, and calorimeter energy-scale uncertainty on the measurement are also listed

W bin (GeV)	$E_{\mathrm{T}}^{\mathrm{CUT}}$ GeV	f	± stat	± sys	± cal
150.0, 180.0	0.5	0.019	± 0.008	$^{+0.015}_{-0.018}$	$^{+0.003}_{-0.003}$
180.0, 210.0		0.013	± 0.002	$^{+0.004}_{-0.005}$	$^{+0.003}_{-0.001}$
210.0, 240.0		0.016	± 0.002	$^{+0.006}_{-0.004}$	$^{+0.000}_{-0.002}$
240.0, 260.0		0.021	± 0.002	$^{+0.004}_{-0.003}$	$^{+0.000}_{-0.001}$
150.0, 180.0	1.0	0.032	± 0.009	$^{+0.025}_{-0.023}$	$^{+0.000}_{-0.008}$
180.0, 210.0		0.027	± 0.003	$^{+0.004}_{-0.005}$	$^{+0.001}_{-0.002}$
210.0, 240.0		0.027	± 0.002	$^{+0.006}_{-0.004}$	$^{+0.001}_{-0.002}$
240.0, 260.0		0.028	± 0.002	$^{+0.005}_{-0.003}$	$^{+0.004}_{-0.001}$
150.0, 180.0	1.5	0.077	± 0.014	$^{+0.068}_{-0.058}$	$^{+0.000}_{-0.024}$
180.0, 210.0		0.044	± 0.004	$^{+0.005}_{-0.005}$	$^{+0.004}_{-0.001}$
210.0, 240.0		0.045	± 0.002	$^{+0.006}_{-0.007}$	$^{+0.003}_{-0.004}$
240.0, 260.0		0.043	± 0.002	$^{+0.005}_{-0.005}$	$^{+0.002}_{-0.002}$
150.0, 180.0	2.0	0.113	± 0.015	$^{+0.048}_{-0.048}$	$^{+0.000}_{-0.018}$
180.0, 210.0		0.067	± 0.004	$^{+0.013}_{-0.007}$	$^{+0.006}_{-0.000}$
210.0, 240.0		0.069	± 0.003	$^{+0.007}_{-0.006}$	$^{+0.004}_{-0.008}$
240.0, 260.0		0.064	± 0.003	$^{+0.008}_{-0.004}$	$^{+0.003}_{-0.005}$

7 Summary

Dijet photoproduction has been measured for configurations in which the two jets with highest transverse energy are separated by a large rapidity gap. The fraction of events with very little transverse energy between the jets is inconsistent with the predictions of standard photoproduction MC models. The same models with the inclusion of a color-singlet exchange sample at the level of 2%–3% are able to describe the data, including the gap-fraction dependency on $E_{\mathrm{T}}^{\mathrm{GAP}}$, W, x_γ^{OBS} and $\Delta\eta$.

The difference in the model predictions precludes an accurate determination of the color-singlet contribution and its behavior as a function of different kinematic variables such as x_γ^{OBS} or W.

Acknowledgements. It is a pleasure to thank the DESY Directorate for their strong support and encouragement. The remarkable achievements of the HERA machine group were essential for the successful completion of this work and are greatly appreciated. The design, construction and installation of the ZEUS detector has been made possible by the efforts of many people who are not listed as authors. We are indebted to R. Appleby and M. Dasgupta for invaluable discussions and for providing the resummed calculation.

References

1. J.R. Forshaw, P.J. Sutton, Eur. Phys. J. C **1**, 285 (1998)
2. DØ Collaboration, B. Abachi et al., Phys. Rev. Lett. **72**, 2332 (1994)
3. DØ Collaboration, B. Abachi et al., Phys. Rev. Lett. **76**, 734 (1996)
4. DØ Collaboration, B. Abbott et al., Phys. Lett. **440**, 189 (1998)
5. CDF Collaboration, F. Abe et al., Phys. Rev. Lett. **74**, 855 (1995)
6. CDF Collaboration, F. Abe et al., Phys. Rev. Lett. **80**, 1156 (1998)
7. CDF Collaboration, F. Abe et al., Phys. Rev. Lett. **81**, 5278 (1998)
8. ZEUS Collaboration, M. Derrick et al., Phys. Lett. B **369**, 55 (1996)
9. H1 Collaboration, C. Adloff et al., Eur. Phys. J. C **24**, 517 (2002)
10. R.B. Appleby et al., JHEP **612**, 044 (2006)
11. A. Banfi, M. Dasgupta, Phys. Lett. B **628**, 49 (2005)
12. R.B. Appleby, M.H. Seymour, JHEP **309**, 056 (2003)
13. ZEUS Collaboration, M. Derrick et al., Phys. Lett. B **293**, 465 (1992)
14. ZEUS Collaboration, U. Holm (ed.), The ZEUS Detector. Status Report (unpublished), DESY (1993), available on http://www-zeus.desy.de/bluebook/bluebook.html
15. N. Harnew et al., Nucl. Instrum. Methods A **279**, 290 (1989)
16. B. Foster et al., Nucl. Phys. B Proc. Suppl. **32**, 181 (1993)
17. B. Foster et al., Nucl. Instrum. Methods A **338**, 254 (1994)
18. M. Derrick et al., Nucl. Instrum. Methods A **309**, 77 (1991)
19. A. Andresen et al., Nucl. Instrum. Methods A **309**, 101 (1991)
20. A. Caldwell et al., Nucl. Instrum. Methods A **321**, 356 (1992)
21. A. Bernstein et al., Nucl. Instrum. Methods A **336**, 23 (1993)
22. J. Andruszków et al., Preprint DESY-92-066, DESY, 1992
23. ZEUS Collaboration, M. Derrick et al., Z. Phys. C **63**, 391 (1994)
24. J. Andruszków et al., Acta Phys. Pol. B **32**, 2025 (2001)
25. W.H. Smith, K. Tokushuku, L.W. Wiggers, *Proceedings of the Computing in High Energy Physics (CHEP 92)*, (Geneva, Switzerland 1992), C. Verkerk, W. Wojcik (eds.), p. 222, also in preprint DESY 92-150B
26. F. Jacquet, A. Blondel, *Proceedings of the Study for an ep Facility for Europe*, (Hamburg, Germany 1979) U. Amaldi (ed.), p. 391, also in preprint DESY 79/48
27. S. Bentvelsen, J. Engelen, P. Kooijman, *Proc. Workshop on Physics at HERA*, (Hamburg, Germany, DESY 1992) W. Buchmüller, G. Ingelman (eds.), vol. 1, p. 23.
28. S. Chekanov, et al., Eur. Phys. J. C **23**, 615 (2002)
29. S. Catani et al., Nucl. Phys. B **406**, 187 (1993)
30. S.D. Ellis, D.E. Soper, Phys. Rev. **D 48**, 3160 (1993)
31. G. Oderda, G. Sterman, Phys. Rev. Lett. **81**, 3591 (1998)
32. T. Sjöstrand, Comput. Phys. Commun. **82**, 74 (1994)
33. G. Marchesini et al., Comput. Phys. Commun. **67**, 465 (1992)
34. R. Brun et al., *geant3*, Technical Report CERN-DD/EE/84-1, CERN, 1987
35. J.M. Butterworth, J.R. Forshaw, M. Seymour, Z. Phys. C **72**, 637 (1996)
36. J.M. Butterworth, S. Butterworth, Comput. Phys. Commun. **153**, 164 (2003)
37. P. Ryan, Ph.D. Thesis, University of Wisconsin-Madison, 2006 (Unpublished)
38. C. Gwenlan, Ph.D. Thesis, University College London, 2003 (Unpublished)
39. CTEQ Collaboration, H.L. Lai et al., Eur. Phys. J. C **12**, 375 (2000)
40. G.A. Schuler, T. Sjöstrand, Z. Phys. C **68**, 607 (1995)
41. G. Marchesini, B.R. Webber, Nucl. Phys. B **310**, 461 (1988)
42. B. Andersson et al., Phys. Rep. **97**, 31 (1983)
43. A.H. Mueller, W.K. Tang, Phys. Lett. B **284**, 123 (1992)
44. N. Kidonakis, G. Oderda, G. Sterman, Nucl. Phys. B **525**, 299 (1998)
45. J.P. Collins, D.E. Soper, G. Sterman, Nucl. Phys. B **308**, 833 (1988)
46. M.G. Sotiropoulos, G. Sterman, Nucl. Phys. B **419**, 59 (1994)
47. H. Contopanagos, E. Laenen, G. Sterman, Nucl. Phys. B **484**, 303 (1997)
48. J.R. Forshaw, A. Kyrieleis, M.H. Seymour, JHEP **608**, 059 (2006)
49. R.B. Appleby, M.H. Seymour, JHEP **12**, 063 (2002)